submitted to PRB, 10/28/2000

Surface Core Level Shifts of Clean and Oxygen Covered Ru(0001)

S. Lizzit, A. Baraldi, A. Groso
[1] *Sincrotrone Trieste S.C.p.A., S.S. 14 Km 163.5, 34012 Trieste, Italy*

K. Reuter, M.V. Ganduglia-Pirovano, C. Stampfl, M. Scheffler
[2] *Fritz-Haber-Institut der Max-Planck-Gesellschaft, Faradayweg 4-6, D-14195 Berlin-Dahlem, Germany*

M. Stichler, C. Keller, W. Wurth, and D. Menzel
[3] *Physik-Department E20, Techn. Universität München, D-85748 Garching, Germany*

(February 1, 2008)

We have performed high resolution XPS experiments of the Ru(0001) surface, both clean and covered with well-defined amounts of oxygen up to 1 ML coverage. For the clean surface we detected two distinct components in the Ru $3d_{5/2}$ core level spectra, for which a definite assignment was made using the high resolution Angle-Scan Photoelectron Diffraction approach. For the $p(2\times2)$, $p(2\times1)$, (2×2)-3O and (1×1)-O oxygen structures we found Ru $3d_{5/2}$ core level peaks which are shifted up to 1 eV to higher binding energies. Very good agreement with density functional theory calculations of these Surface Core Level Shifts (SCLS) is reported. The overriding parameter for the resulting Ru SCLSs turns out to be the number of directly coordinated O atoms. Since the calculations permit the separation of initial and final state effects, our results give valuable information for the understanding of bonding and screening at the surface, otherwise not accessible in the measurement of the core level energies alone.

I. INTRODUCTION

The interaction of oxygen with transition metal surfaces is of considerable interest. Apart from its model character for adsorbate-substrate interactions, it is important as the first step of oxidation of these surfaces, and because of its involvement in catalytic reactions such as CO oxidation, used e.g. for the decontamination of automobile exhaust gases. Therefore, significant efforts have been made in the last decades to investigate this model process, both from an experimental and theoretical point of view. Oxygen chemisorption on transition metal surfaces is largely discussed in terms of strong covalent bonding between the O $2p$ states and the metal valence d-band, accompanied by an unspecified, but noticeable charge transfer from the substrate to the electronegative adsorbate. However, it is not clear which part of the total electron density could or should be assigned to which atom, so that a clearcut distinction between charge transfer and polarization is not possible[1,2].

In this context, theoretical concepts have been developed that try to partition a calculated total electron density into contributions from individual atoms[3–6]. Yet, it would also be useful to have an experimentally accesible quantity, which gives information about the nature of the chemical bond or which would even help to quantify the amount of charge transferred. As core levels are relatively compact and are generally assumed not to take part in the bonding itself, core level binding energies provide such a local probe of the changes in the electrostatic potential of an atom in different environments. At surfaces, the core level energies of the substrate atoms are changed relative to the bulk, giving rise to the so-called Surface Core Level Shifts (SCLS), which can be measured both for clean and adsorbate covered surfaces by high resolution core level photoemission spectroscopy[7,8]. However, total SCLSs comprise not only the so-called initial state effects, which reflect the changes in the electronic distribution at the unperturbed surface, i.e. before the excitation of the core hole, but also the final state effects which are due to the different screening capabilities of the already core-ionized system at the surface and in the bulk[9]. Here, a complementary analysis by density functional theory (DFT) is important, because the latter is able to subdivide the total SCLSs into initial and final state contributions.

Such an approach of coupling experiment and theory has already been used to study the SCLSs of clean transition metals[10], and recently also to analyse adsorbate induced SCLSs due to the interaction of O with the Rh(111) surface for the $p(2\times2)$ and $p(2\times1)$ ordered adlayer structures[11]. The present investigation of the O interaction with the Ru(0001) surface aims to compare the chemisorption behaviour of the two surfaces. Further, on Ru(0001) four different ordered O adlayer structures are formed, which span the coverage range from zero up to one monolayer (ML) and are all extensively characterized by LEED experiments[12–15] and DFT calculations[16]. Hence, a much larger experimental data base is available compared to the O/Rh(111) work, which allows to assess much better the agreement between measured and calculated SCLSs. The four ordered oxygen overlayers, which we have prepared and studied besides the clean surface, are the $p(2\times2)$[12], the $p(2\times1)$[13], the (2×2)-3O[14] and the (1×1)-O[15] structure. In all phases, the O atoms sit in hcp hollow sites and the Ru atoms can have up to three O neighbours as shown in Fig. 1.

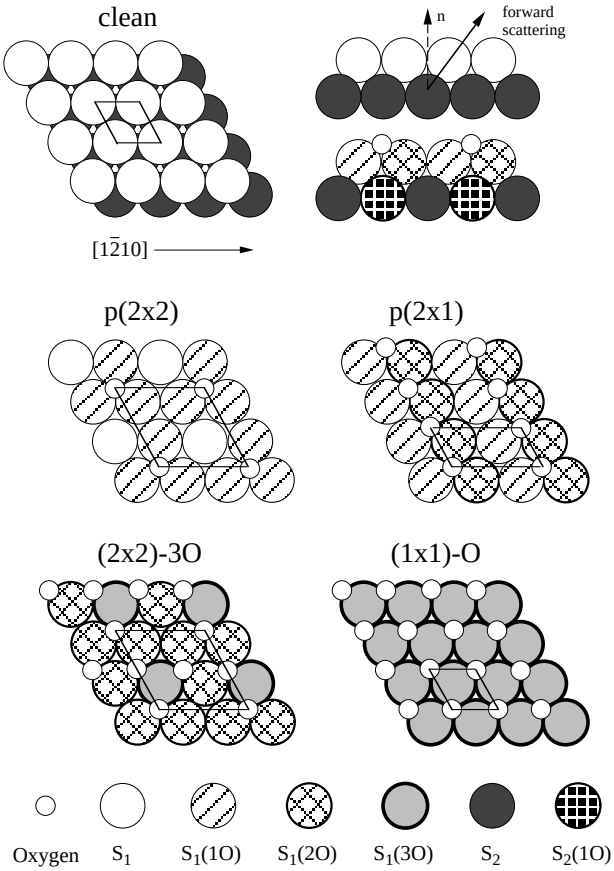

FIG. 1. Periodic oxygen adlayer structures on the Ru(0001) surface with increasing coverage. S_1, S_1(1O), S_1(2O) and S_1(3O) are first layer Ru atoms bound to no, one, two, and three oxygen atoms, respectively. S_2 and S_2(1O) are second layer atoms with no and one oxygen atom directly above on the surface, respectively. The bulk b includes all deeper layer Ru atoms. The top right panel shows sideviews of the clean Ru(0001) surface with an indication of the angle at which strong forward scattering is expected, and of the $p(2 \times 1)$ structure.

As will be shown in section IV A, the Ru $3d_{5/2}$ core level spectra are composed of several peaks, which have to be assigned to certain bonding situations of the corresponding Ru atoms. From the aforementioned work on O/Rh(111), we expect the SCLSs of the first layer atoms to depend primarily on the number of directly coordinated O atoms. The nomenclature that we use to name each of these atoms (and their corresponding SCLS) is derived from this fact and is described in Fig. 1.

If the number of nearest neighbour O atoms is indeed the ruling quantity for the first layer peaks, the assignment of the O-induced components in the spectra is straightforward, because each such peak should be present in two of the considered phases. As shown in Fig. 2, O-induced components at approximately equal positions appear indeed each time at two coverages, so that recurrently working down from the (1×1)-O, the S_1(3O), S_1(2O), and S_1(1O) peaks can directly be assigned. Unfortunately, the situation is not so simple for the S_1 and S_2 peaks, which are both present in the spectrum of the clean surface and of the $p(2\times2)$ phase. While the favorable comparison of experiment and theory to be reported in the present work does also offer an assignment for these peaks, it is still desirable to reach assignments on experimental grounds only. In previous works, high resolution Photoelectron Diffraction in the forward scattering regime had already been successfully utilized to assign different components to first and second layer atoms[17,18]. In this work, a similar strategy will be pursued for the clean Ru(0001) surface, in order to independently assign the remaining S_1 and S_2 components. Once the measurement and the assignment of the various SCLS components has been accomplished, they can be compared with the theoretical results. As the latter allow to separate the final state contribution from the total shift, we are then in a position to discuss the connection of the initial state shift with the nature of the chemical bond.

II. EXPERIMENTAL

The SCLS experiments were performed at the superESCA beamline of the ELETTRA syncrotron facility in Trieste, Italy[19]. The experimental chamber is equipped with a new double pass electron energy analyser (which is composed of two hemispheres of 150 mm radius each)[20] with a 96-channels detector[21] (some earlier results were obtained with a VSW spherical analyser), a VG manipulator (CTPO) with five degrees of freedom and with heating and cooling capabilities (1500 K and 120 K, respectively), a Leybold rear view LEED optics, and a channelplate doser for dosing high amounts of oxygen. All data shown for the series of SCLSs as a function of oxygen coverage were measured in one single run for maximum comparability, but were in good agreement with a partial data set obtained earlier using a VSW 150 mm electron energy analyser with 16 channels parallel detection[22]. The photoelectron diffraction experiment was carried out in a separate run, also using the VSW analyser.

The Ru(0001) crystal was cleaned by Ar^+ sputtering and repeated cycles of oxygen treatments at temperatures ranging from 1000 K to 1200 K. Finally, the sample was flashed to 1500 K and cooled down to 300 K in 1×10^{-7} mbar hydrogen pressure in order to remove any residual trace of oxygen; to remove the hydrogen, the sample was briefly heated to 500 K in UHV before measurements. A very sharp (1×1) LEED pattern with low background intensity was obtained and the XPS did not show any trace of carbon, oxygen, or other contaminants.

The SCLS spectra, both in the measurement of the oxygen structures and in the diffraction experiment, were acquired at a sample temperature lower than 130 K and at a base pressure of 6×10^{-11} mbar. Before doing the

SCLS measurements, the different oxygen structures were defined by observing the intensity of the $(\frac{1}{2},\frac{1}{2})$ spot in the LEED pattern induced by the oxygen adsorption. The fully developed three structures up to 0.75 ML show maxima in the intensity of the extra spots while dosing oxygen when the layer corresponds to 0.25, 0.50 and 0.75 ML coverage. Since the LEED apparatus is mounted in the experimental chamber we could in this way monitor the correct dose of oxygen in order to obtain the desired structure. The coverage was also checked by measuring the O_{1s} intensity. Comparison of the LEED to the XPS data shows that the O_{1s} signal measured at 650 eV photon energy is not much affected by diffraction effects; it therefore gives a good estimate of the relative coverage.

The $p(2 \times 2)$ structure was obtained by exposing the clean Ru(0001) surface to 0.7 Langmuir (nominal) of oxygen at 373 K, and subsequent brief heating to 670 K. The $p(2\times1)$ structure was obtained by dosing onto the $p(2\times2)$ additional 3.5 Langmuir at 373 K, followed again by brief heating to 670 K. As reported in the previous works, flashing at 670 K after the doses is needed to achieve perfect order of the superstructure. The (2×2)-3O structure was obtained by dosing oxygen for 600 seconds with the channel plate doser at a distance of 10 mm from the sample, with a pressure in the chamber of 1.5×10^{-6} mbar at a sample temperature of 600 K. The resulting O_{1s} intensity corresponded to 0.85 ML. In order to remove the excess oxygen the sample was briefly heated to 1060 K; the resulting coverage was 0.77 ML. The (1×1)-O structure was obtained by dosing NO_2 3 times, 800 seconds each, with the doser (pressure in the chamber 5×10^{-8} mbar), at a sample temperature of 600 K. A very sharp (1×1) LEED pattern resulted.

The high resolution Ru $3d_{5/2}$ SCLS spectra were recorded at a photon beam incidence angle of 80° from the surface normal; in the used machine this leads to an electron emission angle of 40°. Three different photon energies, 352, 370 and 400 eV were used in order to change the weight of the core level components due to diffraction and inelastic scattering effects. The $p(2 \times 2)$ structure was measured only at 352 eV. The analyser was operated at 5 eV pass energy with an entrance slit of 2 mm. The combined (photon plus electron) energy resolution is estimated to have been better than 80 meV. For the photoelectron diffraction measurements on the clean Ru(0001) surface, we used a photon energy of 500 eV, which corresponds to a kinetic energy of the Ru $3d_{5/2}$ core level of 220 eV, high enough to have strong forward scattering effects. We performed an azimuthal scan at 40° emission angle with the photon beam now parallel to the surface normal. Since at this high photon energy the cross section for the photoemission is quite low, we used a pass energy of 5 eV in the single pass electron energy analyser, in order to have a good signal to noise ratio, which lowered the overall energy resolution to 120 meV.

III. THEORETICAL

For the density functional theory (DFT) calculations of the SCLSs we employ the generalized gradient approximation (GGA) of the exchange-correlation functional[23], using the full-potential linear augmented plane wave method (FP-LAPW)[24–26] for solving the Kohn-Sham equation. The Ru(0001) surface is modeled using a six layer slab, and O is adsorbed on both sides to preserve mirror symmetry. A vacuum region corresponding to five Ru interlayer spacings (≈11Å) was employed to decouple the surfaces of consecutive slabs in the supercell approach. Within a (2×2) surface unit cell, the positions of all O adatoms and Ru atoms in the outer two substrate layers were fully relaxed for all coverages considered. The resulting adsorption geometries are in very good agreement with existing LEED data[12–15], as well as with earlier DFT pseudo-potential calculations[16].

The FP-LAPW basis set is taken as follows: $R_{\rm MT}^{\rm Ru}$ =2.3 bohr, $R_{\rm MT}^{\rm O}$ =1.3 bohr, wave function expansion inside the muffin tins up to $l_{\rm max}^{\rm wf} = 12$, potential expansion up to $l_{\rm max}^{\rm pot} = 4$. The Brillouin zone integration for the (1×1) cells was performed using a $(12\times12\times1)$ Monkhorst-Pack grid with 19 **k**-points in the irreducible part. For the larger surface cells, the grid was reduced accordingly, in order to obtain the same sampling of the reciprocal space. The energy cutoff for the plane wave representation in the interstitial region between the muffin tin spheres was 17 Ry for the wave functions and 169 Ry for the potential.

The SCLS, $\Delta_{\rm SCLS}$, is defined as the difference in energy which is needed to remove a core electron either from a surface or from a bulk atom:

$$\Delta_{\rm SCLS} = \left[E^{\rm surface}(n_c-1) - E^{\rm surface}(n_c)\right] - \\ - \left[E^{\rm bulk}(n_c-1) - E^{\rm bulk}(n_c)\right] \quad , \qquad (1)$$

where $E^{\rm surface/bulk}(n_c)$ is the total energy of the system considered as a function of the number of electrons, n_c, in a particular core level, c, of a surface or bulk atom respectively[9]. Within the initial state approximation, $\Delta_{\rm SCLS}^{\rm initial}$ is given by

$$\Delta_{\rm SCLS}^{\rm initial} \approx -\left[\,\epsilon_c^{\rm surface}(n_c) - \epsilon_c^{\rm bulk}(n_c)\,\right] \quad . \qquad (2)$$

Here, $\epsilon_c^{\rm surface}$ and $\epsilon_c^{\rm bulk}$ are the Kohn-Sham eigenvalues of the particular core state, c, so that in this approximation the SCLS is simply due to the variation of the orbital eigenenergies before the excitation of the core electron. A full calculation of the ionization energy, which includes the screening contributions from the valence electrons in response to the created core hole, can be achieved by calculating the total energy of an impurity with a core hole in the selected core state. The SCLS is then the difference of two total energies, with the impurity once located at the surface and once inside the bulk[27]. To a good approximation, this difference can also be obtained via the Slater-Janak transition-state approach of evaluating total energy differences[28]. Using the mean value theorem of integration,

$$E(n_c - 1) - E(n_c) = \int_{n_c}^{n_c - 1} \frac{\partial E(n')}{\partial n'} dn' \approx$$
$$\approx -\epsilon_c(n_c - 1/2) \quad , \qquad (3)$$

eq. (1) can be cast into the form of eq. (2), yet this time with a core level occupation of $n_c - 1/2$. Note that this latter approach, from which we derive what we will henceforth call the total SCLS, takes both initial and final state effects (in the spectroscopic sense) into account, so that the results can be compared with the experimental values.

Whereas initial state SCLSs can directly be obtained from our normal all-electron scheme, the total SCLSs require a self-consistent impurity calculation, where one atom is ionized by removing half an electron from the considered core level. We used (2×2) supercells to surround each such atom with neighbours possessing the normal core configuration and kept the fully relaxed ground state geometry fixed. In order to describe an electronically fully relaxed final state, suitable for a system like Ru with a Fermi reservoir of electrons, overall charge neutrality must be imposed, i.e. half an electron was added at the Fermi level.

Initial state and full calculations for the $3d$ SCLSs were done for each inequivalent Ru atom in the outermost two substrate layers at all experimentally described coverages. The bulk core level position, $\epsilon_c^{\rm bulk}$, was calculated using a ten layer bulk slab inside the same supercell as used for the surface calculations, i.e. the previous vacuum region was simply replaced by additional Ru layers. With this procedure an identical sampling of reciprocal space was achieved for both surface and bulk calculations. Having evaluated both the initial state and the total SCLS allows to extract the screening contribution, which is not accessible from the experimental data.

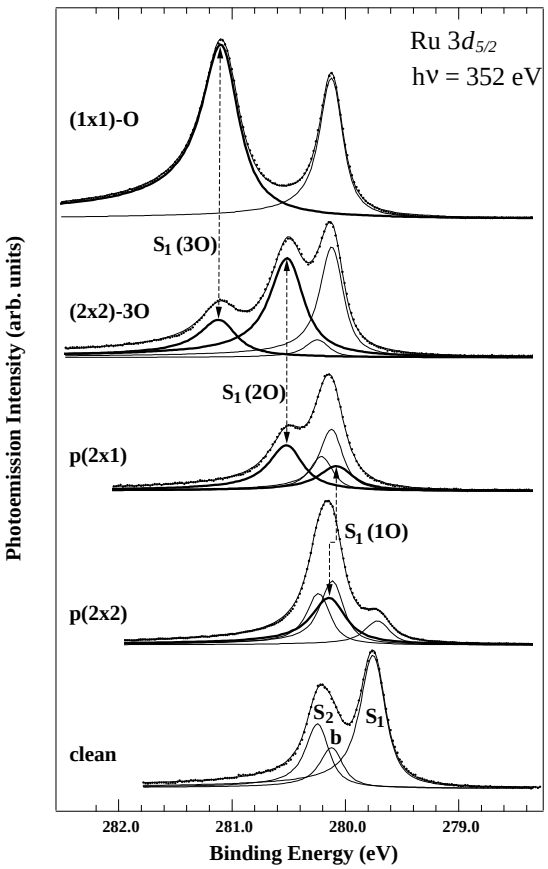

FIG. 2. Ru $3d_{5/2}$ core level spectra for the clean surface and the four oxygen structures. The dots represent the experimental results, while the line in between is the result of the fit. The spectra were measured at a temperature lower than 130 K. The components used in the fit are added in the figure. The curves with the thin line denote the "clean" components (S_1, S_2), while the thicker lines are the oxygen related components, S_1(1O), S_1(2O), and S_1(3O), corresponding to first layer Ru atoms bonded to one, two and three oxygen atoms respectively (cf. Fig. 1). The dashed lines with arrows denote the presence of each of these components in two different structures.

IV. RESULTS

A. SCLS analysis

In Fig. 2 the SCLS spectra measured at 352 eV are shown, together with the fits and the various components. The data were fitted using Doniach-Sunjic functions convoluted with Gaussian broadening[29]. The background was assumed to be linear. In order to get physically meaningful results from the fits it was necessary to put constraints on some parameters of the fitting function as many components have significant overlap. The three spectra at different photon energy of a certain structure (except for the $p(2 \times 2)$) were hence fitted together with identical parameters, leaving free only the intensities of the core level components. In this way the line shape parameters found (Gaussian and Lorentzian width, as well as the asymmetry parameter) are more reliable. Two strategies were then employed to assign the various peaks to the differently coordinated Ru atoms in the surface:

(i) Strategy (i) is an independent experimental assignment, which uses only the structural knowledge of the various O phases as described above. Recurrently working down in coverage starting from the (1×1)-O/Ru(0001) phase, all peaks can thus uniquely be identified with the notable exception of the assignment of the S1 and S2 peak of the clean surface. The latter determination was achieved by supplementary photoelectron diffraction experiments, which will be described in the next subsection.

(ii) Strategy (ii) relies partially on information from our theoretical calculations, the main difference being the inclusion of (small) non-zero shifts of the S_2(1O) peak, which was neglected in strategy (i) to avoid overfitting. As will be discussed in section IV C, approach (ii) improves the quantitative agreement between theory and

TABLE I. Measured SCLSs of the Ru $3d_{5/2}$ level at all coverages in meV. Positive shifts reflect a more strongly bound core level at the surface compared to the bulk. The nomenclature for the different substrate atoms (S_1, S_2 etc.) follows that of Fig. 1. In strategy (i) the value of the S_2(1O) was set to 0 for all the structures, while only for the (1×1)-O its value was obtained by fitting strategy (ii).

	strategy (i)	strategy (ii)
clean, S_1	-366 ± 10	-360 ± 10
clean, S_2	$+125 \pm 10$	$+127 \pm 10$
$p(2 \times 2)$, S_1	-400 ± 20	
$p(2 \times 2)$, S_1(1O)	$+20 \pm 30$	
$p(2 \times 2)$, S_2	$+120 \pm 30$	
$p(2 \times 1)$, S_1(1O)	-50 ± 30	
$p(2 \times 1)$, S_1(2O)	$+390 \pm 10$	
$p(2 \times 1)$, S_2	$+88 \pm 30$	
(2×2)-3O, S_1(2O)	$+387 \pm 20$	
(2×2)-3O, S_1(3O)	$+980 \pm 10$	
(2×2)-3O, S_2	$+127 \pm 30$	
(1×1)-O, S_1(3O)	$+960 \pm 10$	$+920 \pm 10$
(1×1)-O, S_2(1O)	0	-60 ± 10

experiment, yet we argue that approach (i) was also important in order to assure that both, measurement and calculation, lead independently to the same conclusions.

Details of these two fitting procedures are described in the appendix, while the SCLS values are collected in Table I. The error bars shown in the table were estimated from the quality of the fits when changing the SCLS in this energy range. Therefore, possible errors related to the oxygen coverage are not included in the table.

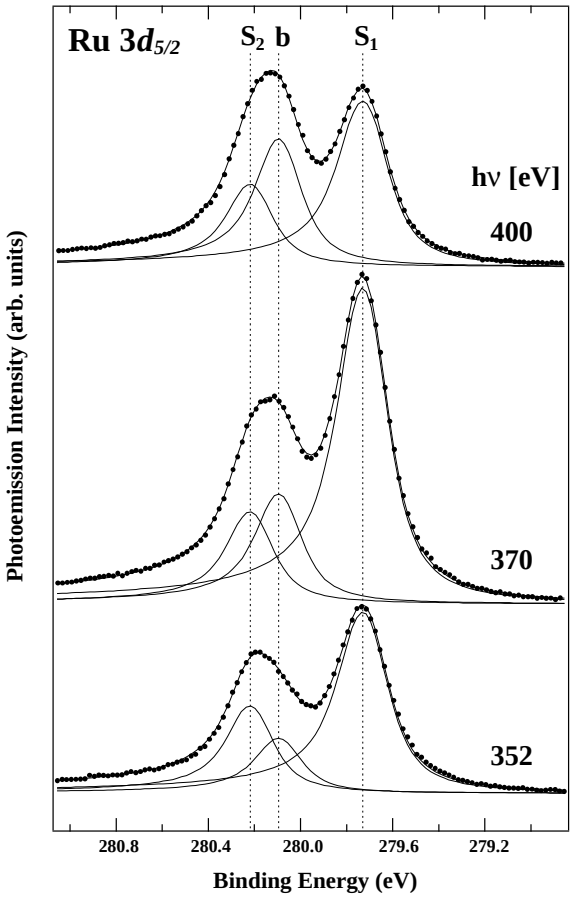

FIG. 3. SCLS spectra of the clean surface measured at different photon energies. The result of the fit is added in the figure as a line crossing the experimental points represented by dots. The three components b, S_1, and S_2 are also added as solid lines. The energy range used to fit the data is wider than what is shown in the figure (see text).

B. SCLS assignment

As already mentioned, the assignment of the oxygen related SCLSs following strategy (i) was implicit in the measurements, whereas that of the clean surface still needs to be proved. In Fig. 3 the three SCLS spectra of the clean surface, measured at the three photon energies given, are shown together with the fits. The spectra have been normalised at the low binding energy side. They have been measured and fitted between 277.9 eV and 281.8 eV in a wider range than shown in the figure. Among the three peaks present, the only one which can be unambiguously assigned is peak b, which belongs to the bulk. This results from the analysis of the SCLSs of the (1×1)-O and is also supported by the fact that when saturating the surface with CO or other adsorbates, the only peak which remained unchanged was peak b.

From a simple inspection of the data it is possible to see that peak b increases at higher photon energy, consistent with a simple mean free path picture. The peak at lower binding energy, S_1, has maximum intensity at 370 eV and the component at higher binding energy, S_2, is more or less constant. From these data it would not be possible to disentangle the various components accounting only for inelastic scattering effects. In fact, the strong modulation of the lower binding energy peak, which will be assigned to the top layer as we show in the following, is mainly due to interference effects, i.e. to photoelectron diffraction, and not to inelastic damping. Therefore we used these interference effects to find the assignment for the clean surface.

The approach relies on the fact that at photoelectron kinetic energies higher than ≈400 eV the conditions for strong forward scattering are fullfilled when an atom of the first layer lies in the line between a second layer emitter atom and the electron energy analyser (cf. Fig. 1, top right panel)[30]. Therefore, changing the azimuthal angle ϕ at an appropriate polar angle θ (for the clean Ru(0001) θ=36°) one should see that the photo-emission intensity of the second layer is strongly modulated due to the forward scattering with the first layer, while the intensity of the peak due to the latter atoms stays almost constant

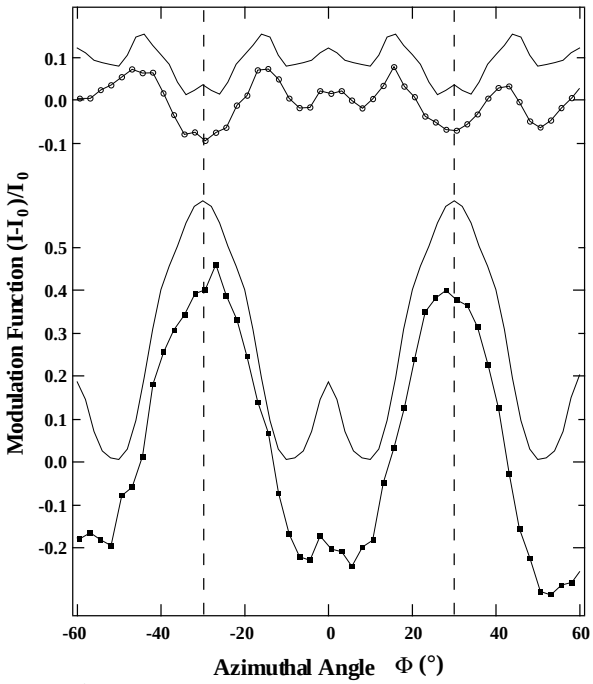

FIG. 4. Angular dependence of the modulation function of the S_1 (open circles) and S_2 (filled squares) components shown in Fig. 3. The S_2 component shows a clear enhancement of the intensity in the forward scattering directions, denoted by the dashed lines in the figure. The solid lines represent the results of multiple scattering simulations. These two curves have been shifted with respect to each other for display purposes.

since no scatterers are present between the emitter in the first layer and the analyser[17]. The problem, which arises in this experiment, is that at such a high kinetic energy and low emission angle, the intensity of the photoemission from the first layers will decrease appreciably with respect to that from the bulk. This will affect much more the S_2 peak, which is very close to the bulk peak, thus becoming almost undetectable.

In order to overcome this problem, we performed preliminary multiple scattering simulations of the first and second layer photoemission intensity. We used the MSCD package developed by Chen and Van Hove[31] which uses multiple scattering theory and the Rehr-Albers separable representation of spherical waves propagators[32]. As input to the program we used the structural parameters obtained from a previous LEED I/V experiment[33]. Moreover, since the Ru(0001) surface is composed by domains rotated by 120° to each other, we summed the photoemission intensity over these domains. At the end we calculated the modulation function defined as $(I(\phi)-I_0)/I_0$, where $I(\phi)$ is the photoemission intensity, while I_0 is its average value. From these calculations we found the best conditions to perform the photoelectron diffraction experiment. In particular, we realized that when performing an azimuthal scan at θ=40° at a kinetic energy of 220 eV, not only the first layer intensity shows pronounced modulations due to the backscattering, but furthermore these are in antiphase with those of the second layer emission in which the characteristic forward scattering peaks are present at ϕ=±30° respect to the $[1\bar{2}10]$ direction. The photoelectron diffraction experimental results together with the multiple scattering simulations are shown in Fig. 4. The agreement between experiment and simulation is very good, hence giving a clear answer to the question we addressed: S_1 belongs to the first layer atoms, while S_2 to those of the second layer.

C. Comparison with theory

Having achieved an unambiguous assignment of all experimentally detected peaks, the next step is to compare these results with the calculated SCLSs. As our intention is to make use of the possibility to decompose the latter shifts into initial and final state contributions, the agreement between theory and experiment should not only be on a qualitative or semi-quantitative level, but should convincingly make clear that there are no inconsistencies whatsoever between both data sets.

In order to perform such a comparison, we first address the accuracy of the DFT calculations. Possible numerical errors can arise due to the use of a finite basis set, as well as due to the finite size of slab and vacuum region in the supercell approach. To assess the effect on the derived SCLS values, we sequentially increased the corresponding values and monitored the SCLSs of both first and second layer atoms of the clean and (1×1)-O covered surface, which form the lower and upper bound of the coverage sequence considered. We checked the convergence of the basis set by increasing the plane wave cutoff in the interstitial from 17 Ry to 23 Ry, as well as using denser **k**-meshes up to a $(18 \times 18 \times 1)$ grid with 37 **k**-points in the irreducible wedge. In both cases the SCLS changes were within ±10 meV. As the SCLSs result from a difference between a surface and a bulk quantity, the obvious point here is to use exactly the same basis set in both calculations, which then leads to a good cancelation of errors and thus makes the SCLS value itself less sensitive to the finite FP-LAPW basis set used.

The main source of error due to the supercell approach stems from the use of slabs of finite thickness. Test calculations performed with ten layer slabs revealed changes in the SCLSs up to ±20 meV, particularly in the second layer shifts. As the changes in the calculated work function were of the same order, we assign these differences to slight variations of the Kohn-Sham potential due to a quantum size effect in the finite slab. On the other hand, further increasing the vacuum region did not have any influence on the SCLS values ($<$ ±5 meV). Summarizing both the errors due to the basis set and the supercell approach, we hence give a conservative estimate of the numerical accuracy of ±30 meV, which is of the same or-

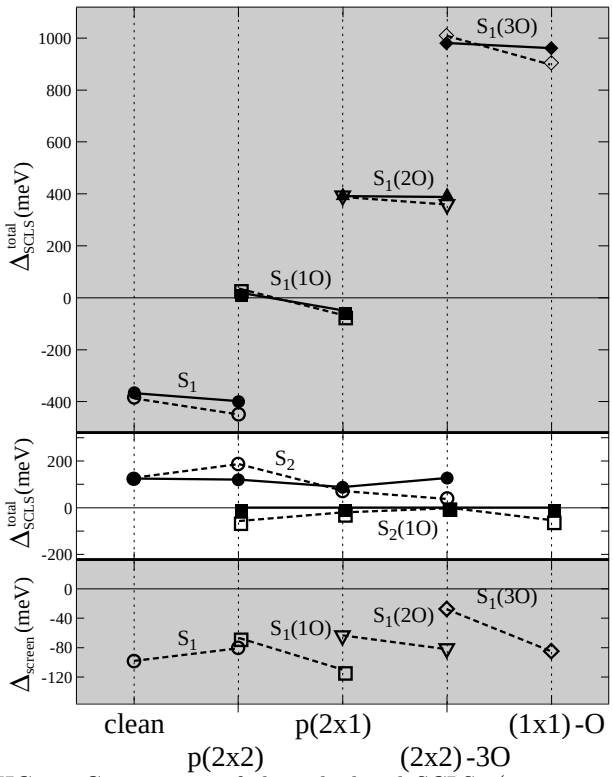

FIG. 5. Comparison of the calculated SCLSs (open symbols) with the experimental results (filled symbols) obtained by fitting strategy (i). The top panel represents the SCLSs of the first substrate layer Ru atoms, while the middle panel displays the SCLSs of the second layer ones. The bottom panel displays the screening contribution to the total first layer shifts.

der as the experimental error, thus justifying the chosen setup.

However, this error estimate does not comprise possible errors due to general deficiencies of the approach, i.e. due to the selected exchange-correlation potential or the use of the transition-state concept to evaluate the total shifts. To this end, we also calculated the SCLSs for both (1×1) phases using the local density approximation (LDA) for the exchange-correlation functional[34]. We found the S_1 and S_2 of the clean surface, as well as the $S_2(1\mathrm{O})$ of the (1×1)-O phase to lie within ± 10 meV of the values obtained with the GGA. On the other hand, the SCLS of the threefold O coordinated first layer atom $S_1(3\mathrm{O})$ changed by 101 meV, significantly worsening the agreement with the experimental value. We attribute this finding to an improved description within the GGA, which – as deduced from the remarkable agreement between experiment and theory reported below – seems to allow a highly accurate determination of the quantity of interest to our study.

Figure 5 shows a comparison between the calculated and the measured SCLSs. It is immediately obvious that almost all theoretical and experimental shifts fall within their mutually assigned error bars, reflecting the consistency between both data sets we aim at. While still showing a good semi-quantitative agreement, only the following shifts do not meet this requirement: S_2 and $S_2(1\mathrm{O})$ in the $p(2\times2)$, S_2 in the (2×2)-3O, as well as $S_1(3\mathrm{O})$ and $S_2(1\mathrm{O})$ in the (1×1)-O. The disagreement in the $S_2(1\mathrm{O})$ shifts is not surprising, as this component was neglected in the original experimental data analysis (strategy (i), cf. section IV A) in order to avoid overfitting. After the theoretical calculations had predicted non-vanishing $S_2(1\mathrm{O})$ shifts particularly for the $p(2\times2)$ and the (1×1)-O phases, the experimental data set was reanalyzed including this component (strategy (ii)). This was unambiguously possible in the case of the (1×1)-O phase with its clearly separate bulk and surface peaks. The resulting value of $S_2(1\mathrm{O}) = -60 \pm 10$meV agrees perfectly with the theoretical $S_2(1\mathrm{O}) = -53 \pm 30$meV, bringing now also the calculated and measured $S_1(3\mathrm{O})$ peak into consistency (theory: $+899 \pm 30$meV, exp: 920 ± 10meV). Unfortunately, the crowding of peaks around the bulk peak in the $p(2 \times 2)$ phase did not allow to add yet another component to the fitting procedure. Hence, we were not able to resolve the small discrepancy for the $S_2(1\mathrm{O})$ peak in this phase.

This leaves only the S_2 components in the $p(2 \times 2)$ and in the (2×2)-3O. As just discussed, the experimentally derived value for the $p(2 \times 2)$ could be affected by neglecting the $S_2(1\mathrm{O})$ peak in the fitting procedure. Additionally, this structure was measured only at 352 eV, and furthermore probably the error bar of the measured SCLS is bigger due to the presence of many peaks in a very small energy range. This can then certainly account for the small difference of 67 meV between calculated and measured shift. Yet, these reasons do not apply in the case of the (2×2)-3O, where theory predicts a vanishing $S_2(1\mathrm{O})$ shift and which was measured at three photon energies. Here, however the weight of the S_2 component is quite small compared to the others, thus increasing the error in the experimental determination of its position. Under these circumstances we do not consider the small difference of 88 meV between theoretical and experimental shift to reflect a significant inconsistency. In conclusion, we hence find both data sets to be fully compatible with each other.

V. ANALYSIS

A. Screening effects

While a main idea behind the study of SCLSs is to gain an understanding of the electronic and structural environment of atoms at the unperturbed surface, i.e. before the core excitation, the measured shifts comprise an additional component, which is due to the different screening capabilities of the core-ionized system at the surface

TABLE II. Calculated Ru 3d SCLSs for the first layer atoms at various coverages. Shown are the total shifts, as well as their decomposition into screening and initial state parts: $\Delta^{\rm total}_{\rm SCLS} = \Delta_{\rm screen} + \Delta^{\rm initial}_{\rm SCLS}$. The rightmost column contains the initial state shifts as obtained for Ru bulk truncated geometries. Units are meV.

	Total	Screening	Initial (relaxed)	Initial (bulk-trunc.)
clean, S_1	-383	-98	-285	-338
$p(2\times2)$, S_1	-448	-80	-368	-407
$p(2\times2)$, S_1(1O)	+36	-65	+101	+42
$p(2\times1)$, S_1(1O)	-67	-111	+44	-12
$p(2\times1)$, S_1(2O)	+395	-62	+457	+454
(2×2)-3O, S_1(2O)	+362	-80	+442	+476
(2×2)-3O, S_1(3O)	+1010	-27	+1037	+1088
(1×1)-O, S_1(3O)	+899	-85	+984	+1072

TABLE III. Calculated Ru 3d SCLSs for the second layer atoms at various coverages. Shown are the total shifts, as well as their decomposition into screening and initial state parts: $\Delta^{\rm total}_{\rm SCLS} = \Delta_{\rm screen} + \Delta^{\rm initial}_{\rm SCLS}$. Units are meV.

	Total	Screening	Initial
clean, S_2	+124	-72	+196
$p(2\times2)$, S_2	+187	-19	+206
$p(2\times2)$, S_2(1O)	-57	-82	+25
$p(2\times1)$, S_2	+72	-34	+106
$p(2\times1)$, S_2(1O)	-21	-96	+75
(2×2)-3O, S_2	+39	-44	+83
(2×2)-3O, S_2(1O)	+3	-35	+38
(1×1)-O, S_2(1O)	-53	-83	+30

and in the bulk[9]. In fact, this screening capability is closely related to the electronic hardness and the surface chemical activity (see e.g. Stampfl et al.[35] and references therein); thus, also this information is of significant interest. Fortunately, calculations as applied in this work provide the possibility to separate the total (measured) shifts into the initial state and the additional final state (i.e. screening) contributions. Table II lists these components for all first layer atoms at the coverages considered. We see that the magnitude of the screening correction is rather small compared to the overall trend in the initial state shifts. Although it leads to an enhanced difference in the total shifts of equally coordinated Ru atoms particularly in the case of the S_1(1O) and S_1(3O) atoms, it still does not overshadow the clear dependence on the number of direct O neighbours, cf. Fig. 5. However, this does not imply that it could be neglected, as only the full shifts lead to the good agreement with the experimental data described above: The initial state shifts alone fall far out of the experimental error bars. Note that especially in the case of the small total shifts corresponding to singly O-coordinated Ru surface atoms, the screening contribution is even larger in magnitude than the initial state shift.

This is even more so for the small total shifts connected to second layer Ru atoms (S_2 and S_2(1O)). Here, the screening correction is of the same order of magnitude as the initial state shift itself ($\approx$ 100 meV), and similar to the trend found for the first layer atoms always negative in sign (cf. Table III). As all initial state S_2 and S_2(1O) are found to be positive, frequent sign changes are hence introduced by the screening contribution. Consequently, in the measurement the second layer shifts can lead to small peaks in close vicinity on *either side* of the bulk peak, which will be hard to resolve experimentally. As is apparent from the two fitting procedures employed in the present experimental analysis (cf. section IV A), this can then indirectly also influence the assessment of the larger first layer shifts. Given that the latter are typically the ones of primary interest, special care with respect to this point should therefore be exerted in the experimental data analysis.

Methfessel and coworkers have shown that final state effects at clean, true transition metal surfaces are largely due to intra-atomic d-electron screening[10,36,37]. Upon core excitation, the d-DOS shift to lower energies causes a valence electron from the Fermi reservoir to restore local charge neutrality by filling up formerly unoccupied d-states. Due to the lowered coordination at the surface, the local density of d-states (d-DOS) is narrower in energy compared to the d-DOS of a bulk atom. Because the total number of states in a band is conserved, already in the simplest rectangular d-band model with a constant d-DOS[38] one would then expect the d-DOS value at and above the Fermi level to be enhanced compared to the bulk situation. This is schematically shown in Fig. 6. In turn, this enhancement implies that the core hole be more efficiently screened at the surface, which in our present sign convention leads to a negative screening correction. In Fig. 7 we show the real self-consistent 4d-DOS, calculated inside the muffin tin spheres[39] for the two limiting phases of the considered coverage range, i.e. the clean and the (1×1)-O surface. Compared to the bulk situation, we indeed find the clean surface d-DOS to be narrowed in energy and in the energy range at and above the Fermi level it is strongly enhanced. Despite the widening of the d-band caused by the O adsorption (see below), this enhancement prevails also for all O covered surfaces, exemplified in Fig. 7 with the (1×1)-O phase. Consequently, negative screening contributions are found throughout the whole coverage sequence.

It is interesting to compare this situation to the work for O adlayers on Rh(111)[11]. There, a sign change in the screening contribution was found, with the lower coverage surfaces screening again better than the bulk, but the higher O-covered surfaces screening worse (cf. Fig. 8). This is connected to the fact that in Rh, which is situated just right of Ru in the periodic system, the Fermi level is located at a different position in the 4d-band. Above that position, the d-DOS is lowered so strongly upon O adsorption that it eventually falls below the value of the bulk d-DOS and thus induces the sign change in the screening correction. In Ru on the other hand, this low-

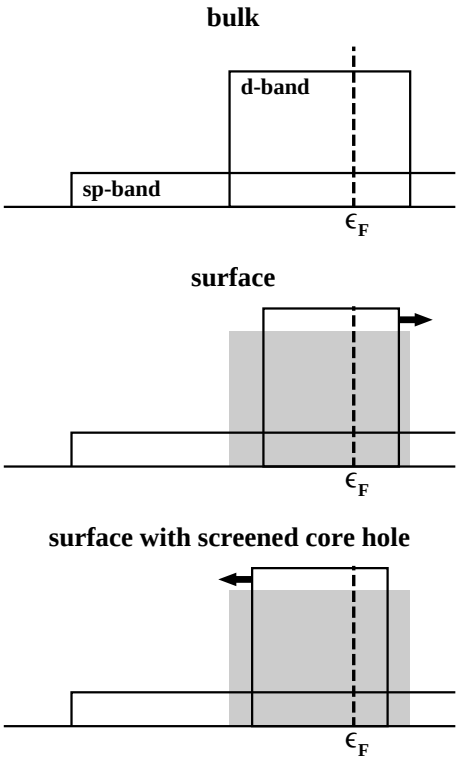

FIG. 6. Schematic DOS in the rectangular d-band model (for the case of a more than half full d-band). At the surface the d-band is narrowed and shifted up in energy to maintain local charge neutrality. Upon core excitation the d-DOS shifts to lower energies and a valence electron from the Fermi reservoir restores local charge neutrality by filling up formerly unoccupied d-states. The enhancement of the surface d-DOS at and above the Fermi level leads to a more efficient screening at the surface and hence to a negative screening contribution to the total SCLS. Note that in the case of a less than half full d-band the d-DOS is shifted down in energy due to the narrowing and hence a negative initial state contribution to the SCLS results. However, the enhancement of the d-DOS at and above the Fermi level nevertheless leads to a negative screening contribution.

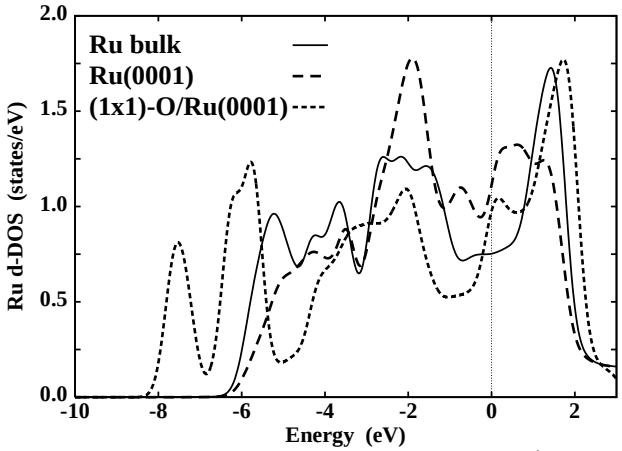

FIG. 7. Calculated 4d-DOS for bulk Ru atoms (solid line) and for first layer Ru(0001) atoms of the clean (dashed line) and (1×1)-O covered surface (dotted line). The energy zero is at the Fermi level.

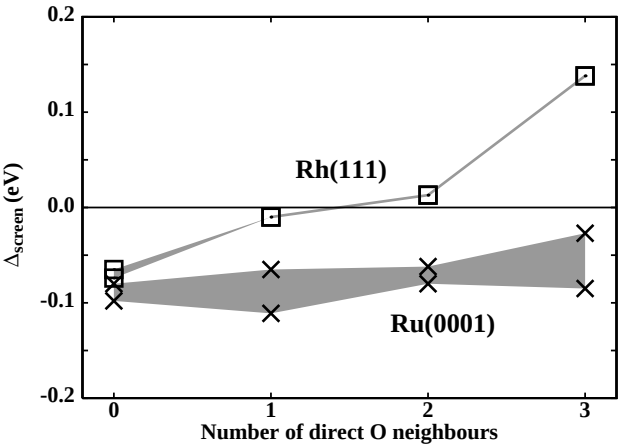

FIG. 8. Comparison of the screening contribution, $\Delta_{\rm screen}$, for O/Ru(0001) (crosses) and O/Rh(111) (boxes) as a function of the number of directly coordinated O atoms. The shaded area is drawn to guide the eye. The O/Rh(111) data is taken from[11].

ering never reaches the bulk d-DOS, so that the screening remains negative in sign throughout (cf. Fig. 8).

B. Initial state shifts

Having subtracted off the final state effect from the total SCLSs, we are now in a position to discuss the initial state contribution, i.e. the change in the local (near nucleus) electrostatic field (see below). For clean transition metals, these shifts are well understood in terms of the narrowing of the surface valence d-band due to the lowered coordination[9]. In order to maintain local charge neutrality, the center of a less (more) than half full d-band moves down- (up-) wards in energy, which goes hand in hand with an attractive (repulsive) contribution to the Kohn-Sham potential (cf. Fig. 6). This potential change acts on the core electrons as well and induces a positive SCLS for the early and a negative SCLS for the late transition metals. This trend involving a sign change across the series is well confirmed by a number of experimental and theoretical studies[9,10,36,40], into which the here derived negative $\Delta^{\rm initial}_{\rm SCLS}$ for clean Ru(0001) fits nicely.

Upon O adsorption, the O $2p$ level interacts with the localized Ru 4d states, causing the formation of bonding and antibonding states close to the lower and upper edge of the valence 4d-band respectively (cf. Fig. 7)[2]. The ensuing increased width of the valence band requires then again an adjustment of the center of gravity of the band in order to maintain local charge neutrality. In the following we will show that this adjustment moves the band downwards in energy and the corresponding attractive contribution to the Kohn-Sham potential is reflected in

TABLE IV. Shift of the center of gravity, ΔC_{4d} in meV, and relative change in the width, ΔW, of the Ru valence $4d$-band for all first layer atoms at the coverages considered with respect to the bulk situation. Additionally shown in the middle column is the shift of the center of gravity resulting from a simple rectangular d-band model as described in the text.

	ΔC_{4d}	$\Delta\tilde{C}_{4d}$ (model)	ΔW
clean, S_1	-200	-200	-12%
$p(2\times2)$, S_1	-180	-180	-11%
$p(2\times2)$, S_1(1O)	0	+30	+2%
$p(2\times1)$, S_1(1O)	-20	+50	+3%
$p(2\times1)$, S_1(2O)	+140	+220	+13%
(2×2)-3O, S_1(2O)	+160	+250	+15%
(2×2)-3O, S_1(3O)	+480	+480	+29%
(1×1)-O, S_1(3O)	+410	+480	+29%

more and more positive SCLSs with increasing O coverage. Further, as the width is connected to the formation of bonds, which obviously scale with the number of directly bound O atoms, similar SCLSs result for equally O coordinated Ru atoms.

In order to quantify this trend, we have evaluated the first and second moment of the valence $4d$-band for each first layer atom at the coverages considered. The pth moment of the DOS, $N(\epsilon)$, is defined as[41],

$$\mu_p \;=\; \int\; N(\epsilon)\;\epsilon^p\;d\epsilon \quad , \tag{4}$$

where in our case $N(\epsilon)$ is the DOS of the Ru $4d$ states[39,42]. μ_0 gives the total number of states in the band and $\mu_1/\mu_0 = \epsilon_{4d}$ its center of gravity. Having obtained these moments for all coverages and for the bulk, allows us then to calculate the shift of the band, $\Delta C_{4d} = \epsilon_{4d}^{\rm bulk} - \epsilon_{4d}^{\rm surf}$, with respect to the bulk situation. The second moment, μ_2/μ_0, is proportional to the mean square width, W^2, of the band which we again translate into relative width changes, $\Delta W = W^{\rm surf}/W^{\rm bulk} - 1$, with respect to the bulk situation. As shown in Table IV, the not O coordinated S_1 atoms possess a band which is 12% narrower than the bulk one, and correspondingly it is shifted by ≈ 0.2 eV to higher energies (cf. Fig. 7). On the other hand, the threefold O coordinated S_1(3O) atoms have a band, which is 29% wider than the one of bulk Ru atoms and its center of gravity is hence shifted by ≈ 0.5 eV to lower energies (cf. Fig. 7).

To gain a *qualitative understanding* in how far the observed shift of the center of gravity is due to the different band width, we next considered the simplistic rectangular d-band model, i.e. a box of constant d-DOS (cf. Fig. 6)[38,41]. In this model ϵ_{4d} is exactly in the middle of the band, i.e. it is $W/2$ above the band bottom, $\epsilon_{4d} = \epsilon_{dn} + W/2$. When this box is positioned with respect to the Fermi level so as to achieve an ideal 70% filling of the Ru $4d$-band, i.e. when we impose local charge

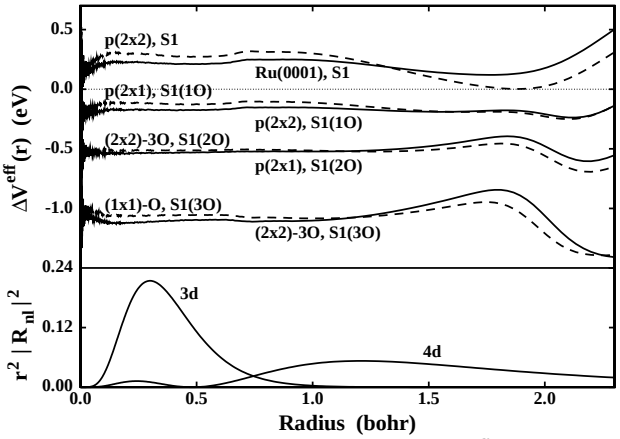

FIG. 9. Top panel: Potential shift, $\Delta V^{\rm eff}(r)$, inside all first layer Ru muffin tin spheres for the various coverages considered. Bottom panel: Radial part of the wavefunction, $r^2\,|R_{nl}(r)|^2$, for the $3d$ and $4d$ orbitals of bulk Ru.

neutrality ($\epsilon_{dn} = -0.7W$, because the Fermi level is our energy zero), then the width, W, of the box and its center of gravity, ϵ_{4d}, are related via,

$$\epsilon_{4d} = -\frac{2}{10}W \quad . \tag{5}$$

With the help of eq. (5), the value of the bulk center of gravity derived from the calculated first moment determines the corresponding width and with this the complete projection of the self-consistent bulk d-DOS onto the rectangular model[43]. After that, the differential form of eq. (5) allows to convert the calculated relative width changes, ΔW, shown in Table IV, into relative shifts of the center of gravity compared to the bulk situation. The resulting shifts, $\Delta\tilde{C}_{4d}$, are given in the middle column of Table IV and match very well the ones obtained directly from the first moment of the real d-DOS. This confirms that the main driving force behind the observed $4d$-band shift, first up in energy for the clean surface and then lower and lower in energy upon increased O coordination, is indeed the notion to preserve local charge neutrality upon a changing d-band width.

The shift of the d-band center is accompanied by a corresponding shift of the Kohn-Sham potential, which in turn is felt by the core electrons and gives rise to the initial state contribution to the SCLSs. In Fig. 9 we show the spherically symmetric part of this potential shift, $\Delta V^{\rm eff}(r)$,

$$\Delta V^{\rm eff}(r) \;=\; V^{\rm eff}_{\rm surf}(r) - V^{\rm eff}_{\rm bulk}(r) \quad , \tag{6}$$

as a function of the radial distance, $r = |\mathbf{r} - \mathbf{R}|$, from the nucleus at $\mathbf{R}$. The shift is primarily related to the number of directly coordinated O atoms, starts with positive shifts (more repulsive potential) for the S_1 type atoms and turns into more and more negative shifts for the S_1(1O), S_1(2O) and S_1(3O) atoms (more attractive

potential). Interestingly, $\Delta V^{\rm eff}(r)$ is always almost constant up to about ≈ 1.2 bohr away from the core. Yet, this is the region seen by the $3d$ core electrons, as exemplified by the extension of the $3d$ radial wavefunction for bulk Ru also plotted in Fig. 9. To first order[44],

$$\Delta^{\rm initial}_{\rm SCLS}(3d) \;\approx\; -4\pi \int dr\; \Delta V^{\rm eff}(r) r^2 |R_{3d}(r)|^2 \qquad (7)$$

holds. Given that $\Delta V^{\rm eff} \approx const$ in the region of the $3d$ orbital and the radial wavefunction is normalized, $\Delta^{\rm initial}_{\rm SCLS}(3d) \approx -\Delta V^{\rm eff}$ results. Of course, an analogous relation to eq. (7) holds also for all other deeper lying core levels, whose $r^2|R_{nl}(r)|^2$ are confined to an even more localized region around the nucleus, also within the constant region of $\Delta V^{\rm eff}(r)$. Hence, the different core levels all display roughly similar shifts[36]. Obviously, this is not the case for the $4d$ valence band, which as shown in Fig. 9 has a much larger radial extension. Hence, it reaches well into the region where $\Delta V^{\rm eff}(r)$ is not constant anymore, which is mainly caused by an increased exchange-correlation contribution in this region of lower electron density[44]. In this region also the non-spherical contributions to the Kohn-Sham potential become significant, so that the magnitude of the shift of the center of gravity of the $4d$-band, C_{4d}, and of $\Delta^{\rm initial}_{\rm SCLS}$ will not be similar, while their overall trend is, as is indeed found when comparing the values given in Table IV and Table II respectively.

Having established the relation between the measured SCLS and the local bonding, at least to the degree as it is reflected in the valence d-DOS, let us focus now on the second layer shifts. Here, only the S_2 type atoms of the clean and $p(2\times 2)$ phase display relatively large shifts of ≈ 200 meV, whereas the shifts of all other second layer atoms remain very small (cf. Table III). Evaluating again the first and second moment of the d-DOS for these atoms, we indeed find only the widths for these two S_2 atoms increased by 5% with respect to the bulk value together with a corresponding shift of the $4d$-band center to lower energies, which gives rise to their positive SCLSs. Yet, while the increased width in the case of the first layer atoms can be explained in terms of binding to more and more O atoms, the second layer Ru atoms always have the same number of nearest neighbours as in the bulk. In this respect it is interesting to notice that only the two mentioned S_2 atoms have first layer neighbours, which are not yet bound to any O atom at all and which hence have somewhat unsaturated bonds. We thus argue that these first layer atoms will most likely reinforce their backbond to the second layer atom below, which will then experience stronger binding than in the bulk situation. Note that this is also reflected in the contraction of the first layer distance with respect to the bulk, which is found only for the lower O coverage phases[12,13]. Judged from the width of the d-DOS, cf. Table IV, any Ru atom that has established bonds to at least one O atom will not show an enhanced backbond tendency anymore, which explains why all other second layer atoms display a more or less bulk-like d-DOS width and consequently very small SCLSs.

VI. DISCUSSION

The analysis of the initial state contribution just presented has shown how the core level shifts act as a sensitive probe of the local electronic structure around an atom, i.e. more precisely how the SCLSs are affected by the *formation of bonds* between the O adsorbates and the Ru first layer atoms. Yet, one could also hope to use the SCLSs to gain a deeper insight into the *nature of the chemical bonds* between the atom and its neighbours. Particularly in the case of adsorbates, i.e. unlike bonding partners, it is tempting to address via the SCLSs the question of charge transfer to or from the surface atoms, or in other words the ionic and covalent contributions to the bonding. In the following subsection we will first discuss our point of view on this relation between SCLSs and charge transfer, and will thereafter apply it to interpret the bonding situation in the O/Ru(0001) and O/Rh(111) systems.

A. SCLSs and charge transfer

In the simplest view, charge transfer off (onto) an atomic site leads to a more attractive (repulsive) potential, thereby causing a shift in the core level towards higher (lower) binding energy. In the case of chemisorption of an electronegative species like oxygen, one would hence expect each time more positive SCLSs for the higher O coordinated Ru first layer atoms, S_1(1O), S_1(2O), and S_1(3O) respectively, as we indeed observe. Yet, despite this qualitatively correct trend, the question remains whether the SCLSs could further be used to better quantify the amount of charge actually transferred. Related to this is then also the question whether the total adsorbate-induced shifts could really be attributed solely to charge transfer.

Recent theories of SCLSs[45–47] have tried to separate the total shift into additional factors apart from charge transfer, namely an environmental and a configurational contribution. The former is viewed as arising from embedding the atom into the delocalized valence charge density of all neighbouring atoms. The ensuing overlap of these valence orbitals onto the atomic site influences the Kohn-Sham potential at the nucleus of the core ionized atom and thus contributes to the shift. Note that such a contribution obviously scales with the number of neighbours, i.e. in our case with the number of directly coordinated O atoms. The configurational contribution, on the other hand, arises in transition metals from the hybridization of the valence d-band with sp states below and above the Fermi level. The latter orbitals are much

more diffuse, i.e. the corresponding charge is on average further away from the nucleus. Hence, a slight redistribution of electrons among these levels at the surface can then also influence the potential. For the particular case of ionic adsorbates on metals, also the polarization of the surface, which tries to screen the adsorbate electric field, has been discussed[1,46].

Correspondingly, the total observable shift would then be the net result of all these (partially canceling) contributions. This argument was e.g. employed to explain the very small negative shifts observed for alkali metal adsorbates on W(110) in contrast to the large positive shifts caused by O/W(110)[45,47,48]. Neglecting any other contribution apart from charge transfer, one would in this case infer a much lower ionicity of the electropositive alkali metals compared to the electronegative oxygen[48]. Yet, this picture was contradicted by the more refined analyses taking also environmental and configurational contributions into account[45,47]. In any case, although all these concepts like charge transfer, covalent bonding or polarization are without doubt useful for our understanding, one has also to admit that they are somehow arbitrary (at least to a certain degree): Whether the build-up of charge between a surface atom and an adsorbate is called covalent bonding or polarization of the metallic charge in response to the adsorbate; or whether the overlap of valence orbitals onto other atomic sites is already called charge transfer or not is simply a matter of taste. In view of the analysis presented in the last section, the very large shift of +1269 meV between the S_1 atoms of the clean surface and the threefold O coordinated S_1(3O) of the (1×1)-O phase is simply the consequence of the strong interaction of the O $2p$ orbitals with the metal $4d$ valence band, which gives rise to bonding and anti-bonding states widening the band. That this goes hand in hand with the sequential build-up of charge between the adsorbate and the Ru surface atom can be seen in Fig. 9, where the surface potential shift shows a more and more pronounced inflection in the region further than $\approx$ 1.7 bohr away from the nucleus. Interpreting this to a certain degree as charge transfer to the O atoms would make the core-level analysis compatible with the continuous increase of the work function upon O adsorption[16] and with calculated charge difference density distributions. Yet, a clear assignment of how much charge is really transferred cannot be made on these grounds.

Coming back to the point why alkali metals show much smaller shifts, one has also to take into account their different interaction with a transition metal surface. The strong interaction of the O $2p$ orbitals with the Ru $4d$-band results in a small O-Ru bondlength of $\approx$ 2.0Å. Even the smallest alkali metal, Li, has a bondlength of $\approx$ 2.7Å to Ru, reflecting a much weaker bond. The interaction with the Li s orbital does not affect the d-band width, and leads in turn only to very small SCLSs. Hence, the different magnitudes in the shifts for the aforementioned electropositive and electronegative adsorbates are merely a consequence of the different type of interaction with the surface atoms, irrespective of the applicability of any underlying charge transfer concept. As a conclusion, we point out that SCLSs certainly are a sensitive probe of the local electronic structure around an atom, yet they intricately depend on the details of the interaction present in the system, which has to be properly analyzed for each specific case to understand the observed shifts. Therefore it does not make much sense to compare magnitudes of SCLSs arising in chemically different systems. On the other hand, within one type of chemistry, as e.g. in our case with the same adsorbate on the same substrate only at different coverages, the SCLSs may indeed be used to further describe the bonding situation – even in the more conceptual language of charge transfer.

B. O on Ru(0001) and Rh(111)

In this view, the equal spacing of $\sim$ 400 meV between SCLSs of increasingly higher O-coordinated Ru atoms (S_1, S_1(1O), S_1(2O), and S_1(3O)) suggests that the type of bonding remains the same throughout the whole coverage range studied, or in other words, that the (unspecified) amount of charge transferred to each O atom remains approximately constant. This interpretation is corroborated by an almost unchanged O_{1s} core level position to within $\pm$20 meV. In particular there is no indication of a qualitatively different chemisorption behaviour between the low coverage ($p(2\times2)$ and $p(2\times1)$) and the high coverage ((2×2)-3O and (1×1)-O) phases, that could explain the long-time believed, but only apparent saturation coverage of $\Theta = 0.5$ ML in UHV[13,49]. As was already concluded in previous studies, this saturation arises therefore solely by kinetic hindrance of the O_2 dissociation process[15,16]. Note, that a similar picture was derived in a recent experimental study on the O/W(110) system, which also exhibited O-coordination dependent SCLSs up to $\approx$ 1 eV for the threefold coordinated W atoms[50].

Apart from this large scale trend, the SCLSs reflect also more subtle details of the bonding situation. This can be seen in the differences in the shifts for equally coordinated atoms present at two coverages; e.g. the shifts for the S_1(1O) type atoms in either the $p(2 \times 2)$ or the $p(2 \times 1)$ phase differ by 57 meV (cf. Table II). These small variations can be due to a small redistribution of the charge at the two coverages, which one may interpret as a slightly different ionicity of the bond caused by the increased repulsion in a denser adsorbate mesh[11]. Alternatively, they could be caused by the small differences in the atomic geometries of the two phases. In order to develop a feeling for the separate magnitudes of these two, interrelated effects, we calculated also the SCLSs at all coverages for an artificial bulk truncated Ru surface with the increasing number of O atoms always sitting in hcp sites at a fixed height corresponding to the one we deduced for the $p(2 \times 2)$ relaxed geometry. The related

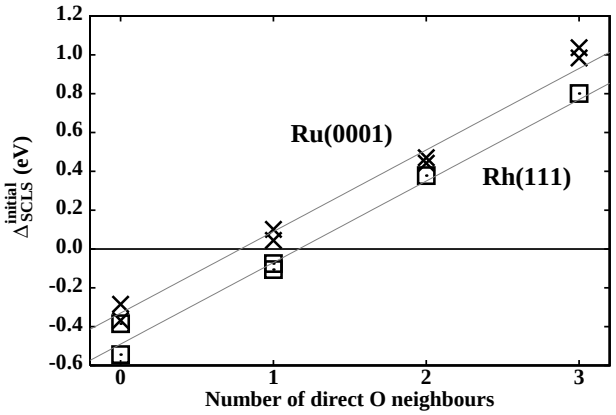

FIG. 10. Comparison of the initial state shifts, $\Delta^{\text{initial}}_{\text{SCLS}}$, for O/Ru(0001) (crosses) and O/Rh(111) (boxes) as a function of the number of directly coordinated O atoms. The lines are drawn to guide the eye. The O/Rh(111) data is taken from[11].

shifts are stated in Table II, indicating that the geometrical changes induced by the adsorbate do amount to small shifts up to about 90 meV. Still, the differences between equally coordinated Ru atoms (now in completely identical nearest-neighbour surroundings for both phases) remain of the same order as before, reflecting now solely the slight charge rearrangement caused by the different adsorbate mesh at the two coverages. In this respect we further note, that this sensitivity of the SCLSs to geometrical differences can also be used to ascertain e.g. the adsorption site. The calculated $\Delta^{\text{total}}_{\text{SCLS}}$ for O in fcc sites on the surface differ by $\approx 100-200$ meV from the ones shown in Table II and are always far outside the experimental error bar. The S_1(3O) shift of a (1×1)-O fcc phase would e.g. be at +718 meV. If there was a significant amount of O sitting in fcc sites at this coverage, it would certainly show up as a shoulder in the experimental spectrum. That this is not the case, cf. Fig. 2, proves that the experimental (1×1)-O phase is nearly perfect hcp, despite the small binding energy difference between both hollow sites[15,16].

Finally, it is interesting to compare the O/Ru(0001) SCLSs to the ones found for O/Rh(111) (same adsorbate, similar transition metal substrates)[11]. Fig. 10 displays the calculated initial state shifts sorted according to the number of directly coordinated O atoms. Apart from the different SCLSs of the clean surfaces caused by the different 4*d*-band filling[9], it is immediately obvious that both materials display almost the same relative O-induced shifts in the whole coverage range considered. The conclusion from these data is hence in line with the one of preceding DFT studies concerning the adsorption energetics[16,51], which apart from the different adsorption site (hcp and fcc on Ru(0001) and Rh(111) respectively) found no qualitative difference in the on-surface O chemisorption behaviour. In particular, in this coverage range there is no hint towards a different catalytic behaviour of both materials at higher O partial pressures[52,53], which hence presumably arises from different oxidation characteristics only after O has started to penetrate into the sample. As a preliminary result from on-going studies concerning this regime, we would like to mention that in contrast to its near constancy in on-surface O phases, we find the O_{1s} core level to be particularly sensitive to variations in the sub-surface O coverage and geometrical position. This suggests that future experimental studies dedicated to sub-surface O and surface oxide formation should focus on this core level, rather than on the metal 3*d*, which we find to somehow saturate at its (1×1)-O value.

VII. SUMMARY

SCLS experiments have been performed on the clean Ru(0001) surface and on the four oxygen ordered adlayer structures which form in UHV, namely the $p(2\times2)$, $p(2\times1)$, (2×2)-3O and (1×1)-O. For the clean surface the high energy resolution photoelectron diffraction approach was used in order to make the assignment of the shifts measured to the corresponding substrate atoms. For the oxygen related SCLSs we find a clear dependence of the SCLS on the number of nearest neighbour O atoms, with the higher O coordinated Ru atoms exhibiting shifts up to 1 eV to higher binding energies. We obtain very good agreement between the experimentally determined SCLSs and first principles calculations, which confirms that within the GGA the latter are able to describe this quantity with high accuracy ($\pm$30 meV). Using the theoretical approach, it was possible to separate the total SCLSs into initial and final state contributions. We found the latter to be mainly due to an enhanced intra-atomic 4*d*-electron screening at the surface, which arises from the increased 4*d*-DOS at and above the Fermi level compared to the bulk situation. The initial state shifts are connected to a varying width of the Ru valence 4*d* band either due to the reduced coordination of the atoms at the surface or to the interaction with the O 2*p* level which causes the formation of bonding and antibonding states widening the band. As the width of the band is connected to the formation of bonds, which scale with the number of directly bound O atoms, similar SCLSs result for equally O coordinated Ru atoms. The almost linear increase of $\Delta^{\text{initial}}_{\text{SCLS}}$ for increasingly higher O coordinated Ru atoms suggests that the type of bonding remains roughly the same over the considered coverage sequence up to the full monolayer, which may be interpreted as an almost constant amount of charge transferred to each electronegative O atom. This finding is similar to the result for O on Rh(111)[11], i.e. both surfaces show a qualitatively similar on-surface chemisorption behaviour. On the other hand the screening properties of both surfaces are different in that the Ru(0001) surface is always able to screen the created core hole better than the bulk while the Rh(111)

surface screens better only for the low coverage O phases.

These results show that a combined experimental and theoretical determination of SCLSs provides valuable insight into the O-metal interaction in different chemical environments. Hence, SCLSs offer a promising tool to study not only the on-surface O chemisorption behaviour of surfaces, but also the transition to sub-surface O and surface oxide formation.

APPENDIX A:

The fit of the experimental data was performed in two different ways, named strategy (i) and strategy (ii). The line shape parameters of the various components are the Lorentzian and Gaussian width, L and G in eV respectively, as well as the asymmetry parameter α.

1. strategy (i)

The fitting procedure strategy (i) is completely independent of the theoretical results and assumes the $S_2(1O)$ component to be indistinguishable from the bulk in all the fits. This assumption rests on the spectrum for the (1×1)-O phase, where the bulk and $S_1(3O)$ are far from each other and the clear-cut two peak spectrum with small overlap in between does not justify a third component hidden under either peak at first glance, cf. Fig. 2.

The approach used to fit the data was the following:

1) First the (1×1)-O structure was fitted, for which only two components were assumed to be present which must be bulk and the $S_1(3O)$. In this way we found the line shape parameters of the bulk (L = 0.175, $\alpha = 0.085$, G = 0.11) and the $S_1(3O)$ (L = 0.31, $\alpha = 0.150$, G = 0.11) peaks.

2) Then we fitted the clean surface. In this case three components are present: S_1, S_2 and bulk. We kept the asymmetry parameter and the Lorentzian width for all components at the values found previously for the bulk in the (1×1)-O, and we let free the Gaussian width of the S_2 and S_1. The Gaussian width of S_2 turns out to be 0.11 eV, the same as for the bulk, while that of S_1 is 0.13 eV. The assignment to first and second layer atoms, shown in Fig. 2, has been corroborated by independent SCLS-photoelectron diffraction experiments as described in section IV B.

3) Next we fitted the spectra at 352 eV of the $p(2 \times 2)$ in order to determine the parameters of the $S_1(1O)$ peak (L = 0.30, $\alpha = 0.085$, G = 0.11). These parameters are not as accurate because of the strong overlap of this peak with that of the bulk and the other peaks present.

4) Then we fitted the $p(2 \times 1)$ spectrum in order to determine the parameters of the $S_1(2O)$ component (L = 0.30, $\alpha = 0.085$, G = 0.11). The parameters for this peak are not as accurate as for the $S_1(3O)$, but are definitely more accurate than those of the $S_1(1O)$.

5) Finally we fitted the $(2 \times 1)3O$ using the line shape parameters found previously for the various components.

2. strategy (ii)

1) In the second strategy the clean surface was fitted first. In the fit we kept the Lorentzian width the same for the three components, letting free the asymmetry and the Gaussian width. Fitted this way, the Lorentzian width is 0.18, the asymmetry turns out to be the same for all components, 0.086, and the Gaussian width of the S_1, S_2 and bulk peak is 0.13, 0.09, and 0.08 respectively. The quality of the fit was slightly better than that of the fit of the clean surface using the first strategy, while the derived SCLSs were almost the same: $S_1 = -360$ meV and $S_2 = +127$ meV.

2)Then we tried to fit the (1×1)-O structure fixing for the bulk peak the same line shape parameters found for the clean surface and assuming that only two components, bulk and $S_1(3O)$, are present. In line with the theoretical prediction, the bad quality of the fit rendered it necessary to fix a third non-zero component, $S_2(1O)$, at slightly lower binding energy than the bulk peak. We fixed for this new peak the same line shape parameters as for the bulk. By fitting the (1×1)-O structure with these three peaks instead of two, the parameters of the $S_1(3O)$ do not change with respect to the first fitting strategy. The bulk and the $S_2(1O)$ components show similar intensities. The SCLS for $S_1(3O)$ and $S_2(1O)$ turn out at 920 meV and -60 meV respectively, both now in excellent agreement with the theoretical values.

3) Similarly, we tried to add a non-zero $S_2(1O)$ peak close to the bulk region for all other structures, but the results were meaningless since too many peaks are present in a small energy range.

[1] J. Bormet, J. Neugebauer, and M. Scheffler, Phys. Rev. B **49**, 17242 (1994).

[2] M. Scheffler and C. Stampfl, *Theory of Adsorption on Metal Substrates*, In: Handbook of Surface Science, Vol. 2: Electronic Structure, (Eds.) K. Horn, M. Scheffler. Elsevier Science, Amsterdam (2000), p. 286.

[3] R.S. Mulliken, J. Chem. Phys. **23**, 1833 (1955).

[4] R. Hoffmann, *Solids and Surfaces: A Chemist's View of Bonding in Extended Structures*, VCH, New York (1988).

[5] R.F.W. Bader, *Atoms in Molecules. A Quantum Theory*, Int. Series of Monographs on Chemistry, Vol. 22, Oxford University Press, Oxford (1990).

[6] A.D. Becke and K.E. Edgecombe, J. Chem. Phys. **92**, 5397 (1990).

[7] N. Mårtensson and A. Nilsson, *High Resolution Core-Level Photoelectron Spectroscopy of Surfaces and Adsorbates*, Springer Series in Surface Science, Vol. 35, (1994) 65.
[8] A. Baraldi, S. Lizzit, and G. Paolucci, Surf. Sci. **457**, L354 (2000).
[9] D. Spanjaard, C. Guillot, M.C. Desjonqueres, G. Treglia, and J. Lecante, Surf. Sci. Rep. **5**, 1 (1985); W. F. Egelhoff, Surf. Sci. Rep. **6**, 253 (1987).
[10] J.N. Andersen, D. Hennig, E. Lundgren, M. Methfessel, R. Nyholm, and M. Scheffler, Phys. Rev. B **50**, 17525 (1994).
[11] M.V. Ganduglia-Pirovano, M. Scheffler, A. Baraldi, S. Lizzit, G. Comelli, G. Paolucci, and R. Rosei, Phys. Rev. B, *submitted*.
[12] M. Lindroos, H. Pfnür, G. Held, and D. Menzel, Surf. Sci. **222**, 451 (1989).
[13] H. Pfnür, G. Held, M. Lindroos, and D. Menzel, Surf. Sci. **220**, 43 (1989).
[14] M. Gsell, M. Stichler, P. Jakob, and D. Menzel, Israel J. Chem. **38**, 339 (1998).
[15] C. Stampfl, S. Schwegmann, H. Over, M. Scheffler, and G. Ertl, Phys. Rev. Lett. **77**, 3371 (1996).
[16] C. Stampfl and M. Scheffler, Phys. Rev. B **54**, 2868 (1996).
[17] S. Lizzit, K. Pohl, A. Baraldi, G. Comelli, V. Fritzsche, E. W. Plummer, R. Stumpf, and Ph. Hofmann, Phys. Rev. Lett. **81**, 3281 (1998).
[18] A. Baraldi, S. Lizzit, G. Comelli, A. Goldoni, Ph. Hoffmann, and G. Paolucci, Phys. Rev. B **61**, 4534 (2000).
[19] A. Baraldi, M. Barnaba, B. Brena, D. Cocco, G. Comelli, S. Lizzit, G. Paolucci, and R. Rosei, J. Electr. Spectroscopy **76**, 145 (1995).
[20] A. Baraldi and V. R. Dhanak, J. Electr. Spectroscopy **67**, 211 (1994).
[21] L. Gori, R. Tommasini, G. Cautero, D. Giuressi, M. Barnaba, A. Accardo, S. Carrato, and G. Paolucci, Nucl. Instr. and Meth. A **431**, 338 (1999).
[22] M. Stichler, Ph.D. thesis, Techn. Universität München (1998).
[23] J.P. Perdew, S. Burke and M. Ernzerhof, Phys. Rev. Lett. **77**, 3865 (1996).
[24] P. Blaha, K. Schwarz and J. Luitz, **WIEN97**, *A Full Potential Linearized Augmented Plane Wave Package for Calculating Crystal Properties*, Karlheinz Schwarz, Techn. Universität Wien, Austria, (1999). ISBN 3-9501031-0-4.
[25] B. Kohler, S. Wilke, M. Scheffler, R. Kouba, and C. Ambrosch-Draxl, Comput. Phys. Commun. **94**, 31 (1996).
[26] M. Petersen, F. Wagner, L. Hufnagel, M. Scheffler, P. Blaha, and K. Schwarz, Comp. Phys. Commun. **126**, 294 (2000).
[27] B. Johansson and N. Mårtensson, Phys. Rev. B **21**, 4427 (1980).
[28] J.F. Janak, Phys. Rev. B **18**, 7165 (1978); J.P. Perdew and M. Levy, Phys. Rev. B **56**, 16021 (1997).
[29] S. Doniach and M. Šùnjić, J. Phys. C **3**, 185 (1970).
[30] D.P. Woodruff and A.M. Bradshaw, Rep. Prog. Phys. **57**, 1029 (1994), and references therein.
[31] Y. Chen and M.A. Van Hove, http://electron.lbl.gov/mscdpack/.
[32] J.J. Rehr and R.C. Albers, Phys. Rev. B **41**, 8139 (1990).
[33] H. Over, H. Bludau, M. Skottke-Klein, G. Ertl, W. Moritz, and C.T. Campbell, Phys. Rev. B **45**, 8638 (1992).
[34] J.P. Perdew and Y. Wang, Phys. Rev. B **45**, 13244 (1992).
[35] C. Stampfl, M.V. Ganduglia-Pirovano, K. Reuter, and M. Scheffler, Surf. Sci. **500**, *submitted*.
[36] M. Methfessel, D. Hennig, and M. Scheffler, Surf. Sci. **287/288**, 785 (1993).
[37] M. Methfessel, D. Hennig, and M. Scheffler, Surf. Rev. Lett. **2**, 197 (1995).
[38] J. Friedel, In: *The Physics of Metals*, (Ed.) J.M. Ziman, Cambridge University Press, Cambridge (1969), p. 340.
[39] We calculate the 4*d*-DOS, $N_{4d}(\epsilon)$, only inside the muffin tin spheres of the FP-LAPW scheme. As can be seen in Fig. 9, the 4*d* orbital extends beyond the currently chosen sphere of 2.3 Bohr radius (equivalent to 91% of half the nearest neighbour distance in bulk Ru). Yet, these tails of the 4*d* orbital hardly affect the shape of $N_{4d}(\epsilon)$, which is what we are primarily interested in. We checked this by reducing the muffin tin radius by 10%. While the calculated 4*d*-DOSs simply contained fewer states, their overall shape was almost unchanged. This is reflected in the computed moments of the DOS, e.g. for the bulk Ru 4*d*-band, where the number of states, μ_0, changes from 7.85 (2.3 bohr) to 6.97 (2.0 bohr), but the center of gravity, ϵ_c, and the width, W, change only by 60 meV and 0.2% respectively. Note particularly that our intention in presenting the 4*d*-DOSs is not to make a quantitative theory, but 'only' to explain our DFT results conceptually.
[40] M. Aldén , H.L. Skriver, and B. Johansson, Phys. Rev. Lett. **71**, 2449 (1993); M. Aldén, I.A. Abrikosov, B. Johannson, N.M. Rosengaard, and H.L. Skriver, Phys. Rev. B **50**, 5131 (1994).
[41] D. Pettifor, *Bonding and Structure of Molecules and Solids*, Clarendon Press, Oxford (1995).
[42] As apparent from Fig. 7, the upper integration limit in eq. (4) is not well defined. We integrated all states up to $\epsilon_{up} = \epsilon_F + 2.5$ eV, which is at all considered coverages above the strong decrease in the *d*-DOS at the top of the band (cf. Fig. 7). While the absolute moments, μ_p, certainly depend on the choice of this upper integration limit, the relative changes in the moments, $\Delta\mu_p = \mu_p(\Theta_1) - \mu_p(\Theta_2)$, for different coverages are not very sensitive to it. We tested this by varying the upper integration limit to either $\epsilon_{up} = \epsilon_F + 2.0$ eV or $\epsilon_{up} = \epsilon_F + 3.0$ eV. The changes in ΔC_{4d} were within ± 60 meV and the ΔWs differed by less than 2%. These variations are small compared to the overall trend which we intend to explain, so that the conclusions drawn with the present limit are independent of the particular choice made.
[43] The values for the rectangular *d*-band model of bulk Ru are determined as: bottom of band, $\epsilon_{dn} = -5.81$ eV, top of band, $\epsilon_{up} = +2.49$ eV, center of gravity, $\epsilon_c = -1.66$ eV, and total band width, $W = 8.30$ eV. The band filling is 70% and the energy zero is the Fermi level.
[44] M.V. Ganduglia-Pirovano, V. Natoli, M.H. Cohen, J. Kudrnovský, and I. Turek, Phys. Rev. B **54**, 8892 (1996).
[45] G.A. Benesh and D.A. King, Chem. Phys. Lett. **191**, 315 (1992).
[46] P.S. Bagus, C.R. Brundle, G. Pacchioni, and F. Parmigiani, Surf. Sci. Rep. **19**, 266 (1993).
[47] P.S. Bagus, F. Illas, G. Pacchioni, and F. Parmigiani, J.

Electr. Spectroscopy **100**, 215 (1999).
[48] D.M. Riffe, G.K. Wertheim, and P.H. Citrin, Phys. Rev. Lett. **64**, 571 (1990).
[49] T.E. Madey, H.A. Engelhardt, and D. Menzel, Surf. Sci. **48**, 304 (1975).
[50] D.M. Riffe and G.K. Wertheim, Surf. Sci. **399**, 248 (1999).
[51] M.V. Ganduglia-Pirovano and M. Scheffler, Phys. Rev. B **59**, 15533 (1999).
[52] C.H.F. Peden and D.W. Goodman, J. Phys. Chem. **90**, 1360 (1986).
[53] C.H.F. Peden, D.W. Goodman, D.S. Blair, P.J. Berlowitz, G.B. Fischer, and S.H. Oh, J. Phys. Chem. **92**, 1563 (1988).